Quantification of *Kras* Mutant Fraction in the Lung DNA of Mice Exposed to Aerosolized Particulate Vanadium Pentoxide by Inhalation

Malathi Banda[1], Karen L. McKim[1], Lynne T. Haber[2], Judith A. MacGregor[3], B. Bhaskar Gollapudi[4], and Barbara L. Parsons[1,5]

[1] Division of Genetic and Molecular Toxicology, National Center for Toxicological Research, US FDA, Jefferson, AR
[2] Toxicology Excellence for Risk Assessment, Cincinnati, OH
[3] Toxicology Consulting Services, Bonita Springs, FL
[4] Exponent, Midland, MI
[5] Corresponding author

Final Report
November 17, 2014

This report is being submitted to Toxicology Excellence for Risk Assessment (TERA) as part of the Cooperative Research and Development Agreement entitled, "Development of a method to use *in vivo* mutagenicity data to address the question as to whether a specific chemical induces cancer via a mutagenic or a non-mutagenic mode-of-action (MOA)."

[5]Barbara L. Parsons
US Food and Drug Administration,
National Center for Toxicological Research,
Division of Genetic and Molecular Toxicology,
HFT-120,
3900 NCTR Road,
Jefferson, AR 72079
Phone: 870-543-7946
Fax: 870-543-7393
Email: barbara.parsons@fda.hhs.gov

ABSTRACT

This study investigated *Kras* mutation as an early event in the development of lung tumors induced by inhalation of particulate vanadium pentoxide (VP) aerosols. A National Toxicology Program tumor bioassay of inhaled particulate VP aerosols established that VP-induced alveolar/bronchiolar carcinomas of the $B6C3F_1$ mouse lung carried *Kras* mutations at a higher frequency than historically observed in spontaneous mouse lung tumors. This study sought to: 1) to characterize any *Kras* mutational response with respect to VP exposure concentration, and 2) determine whether amplification of preexisting *Kras* mutation was an early event in VP-induced mouse lung tumorigenesis. Male Big Blue $B6C3F_1$ mice (6 mice/group) were exposed to aerosolized particulate VP by inhalation, six hours/day, five days/week for four or eight weeks, using VP exposure concentrations of 0, 0.1, and 1 mg/m^3. The levels of two different *Kras* codon 12 mutations (GGT→GAT and GGT→GTT) were measured in lung DNAs by Allele-specific Competitive Blocker PCR (ACB-PCR). The effect of VP exposure on the frequency of *Kras* mutation in lung DNA (left lobe) from exposed mice was evaluated alongside measurement of *cII* (neutral reporter gene) mutant frequency in lung DNA (right lobes) from the same mice. In the initial ACB-PCR analysis, no significant changes in the codon 12 GAT MF were observed in mice exposed to VP compared to the concurrent controls, with the exception of a significantly greater MF in mice exposed to 0.1 mg/m^3 VP for 4 weeks ($P = 0.0163$). In a second independent ACB-PCR analysis of the samples, the MF observed in VP-exposed mice were not significantly different from the concurrent controls at both exposure concentrations (0.1 and 1.0 mg/m3) and time points (4 and 8 weeks). Only a small number of VP-treated

lung DNA samples contained measureable levels of *Kras* codon 12 GTT mutation and no statistically-significant differences among treatment groups were observed. Given that 8 weeks of inhalation of a tumorigenic concentration of particulate aerosols of VP did not result in a significant change in levels of lung *Kras* mutation, the accumulation of *Kras* mutation occurs later during chronic VP exposure and is likely a late event in VP-induced mouse lung carcinogenesis.

Abbreviations: ACB-PCR, Allele-specific competitive blocker-Polymerase Chain Reaction; MOA, mode of action; MF, mutant fraction; NTP, National Toxicology Program; PCR, Polymerase Chain Reaction; VP, vanadium pentoxide; WT, wild-type

INTRODUCTION

The rodent tumor bioassay is used to characterize the tumorigenic potential of chemical and physical agents. Tumor bioassays tend to use doses of test article that are greater than human exposures, necessitating low-dose extrapolation. Low dose linear extrapolation is a default assumption of quantitative cancer risk assessment and is considered appropriate for chemicals that interact with DNA to cause DNA damage and mutation as early key events in carcinogenesis. The option of selecting a nonlinear model for low dose extrapolation may be justified when it is clear that induction of mutation is not an early key event driving tumor development [1]. Consequently, mutational analysis is an important component of cancer risk assessment. Information regarding the timing, magnitude, and dose-relatedness of the mutational response, and

whether a shift in mutational spectra is observed between treated and control animals, are factors that should be considered when trying to understand MOA.

Chemical exposures may increase the mutational burden in a cell, tissue, or whole animal in several ways. Chemicals may directly damage DNA or nucleobases causing mutation through miscoding or misrepair of the damage, and a variety of assays that detect these types of events are available. Chemicals may also impact mutation through an effect on cell survival or proliferation. For example, cytotoxicity and compensatory cell proliferation may amplify the impact of spontaneous mutations. Alternatively, a chemical might cause the replication of pre-existing mutant cells (through an effect on receptor-mediated signaling, for example). There is a dearth of approaches for evaluating chemical impacts on the frequency of mutations that drive cancer (including amplification of pre-existing mutation), particularly in the tumor target tissue.

Recently, a paradigm was developed as a means of distinguishing between chemical-induced *de novo* mutation and chemical-induced amplification of pre-existing mutation [2, 3]. Under this paradigm, the chemical effect in terms of induction of *Kras* mutation is compared to its effect on the induction of neutral reporter gene mutations in DNA isolated from a particular tissue of exposed animals. As part of this paradigm, measurement of *Kras* codon 12 GGT to GTT (G12V) and GGT to GAT (G12D) mutations by Allele-specific Competitive Blocker PCR (ACB-PCR) is employed because: 1) these mutations can occur at levels detectable by ACB-PCR in the DNA isolated from normal rodent and human tissues (particularly G12D) [4], and 2) these mutations are prevalent in multiple types of rodent and human tumors [5]. Selective

induction of a particular mutational specificity in *Kras*, as well as the *lacI* or *cII* transgene of Big Blue rodents, would support a genotoxic mechanism of chemical effect, whereas an increase of both mutations (in proportion to their spontaneous levels), with no shift in the mutational spectra observed in a transgene, would support a mechanism involving amplification of pre-existing mutation. A study of inhaled ethylene oxide (EO) was undertaken using this paradigm. A significant increase in *cII* mutant frequency was observed in lung DNAs of mice exposed to 200 ppm EO [6]. It was also concluded that EO's concentration-dependent effects on *Kras* did not occur through conversion of DNA damage to mutation, based on the observation that *Kras* and *cII* mutation frequencies in individual animals were inversely correlated [3].

In a B6C3F1 mouse chronic inhalation bioassay of VP, an increased incidence of alveolar/bronchiolar adenomas and carcinomas was observed compared to chamber controls [7]. The incidences of alveolar/bronchiolar carcinomas in male mice were 24%, 58%, 60%, and 70% for the 0, 1, 2, and 4 mg/m^3 VP treatment groups, respectively. The incidences of alveolar/bronchiolar adenomas and carcinomas (combined) in males were 44%, 84%, 86%, and 86% for the 0, 1, 2, and 4 mg/m^3 VP treatment groups, respectively. *Kras* mutation was observed in 30% of the alveolar/bronchiolar carcinomas from a pooled historical control group of B6C3F$_1$ mice, whereas *Kras* mutation was observed in 73% of the 40 alveolar/bronchiolar carcinomas examined from VP-treated B6C3F$_1$ mice [7]. Unfortunately, only 2 (sex unknown), of the concurrent control mice from the VP study were studied for *Kras* mutations. Nevertheless, it appears from this observation that *Kras* mutation is part of the etiology of VP-induced lung carcinogenesis, but these data alone do not show whether the

mutation is an early or late event. *Kras* codon 12 GGT to GAT (G12D) mutation was the most prevalent mutation observed in VP-induced alveolar/bronchiolar carcinomas examined, detected in 12/29 (41%) of the tumors identified as *Kras* mutant [7]. The next most prevalent mutation observed in VP-induced alveolar/bronchiolar carcinomas was the *Kras* codon 12 GGT to GTT (G12V) mutation, detected in 7/29 (24%) of *Kras* mutant tumors that were analyzed. Taken together, therefore, these two mutations account for 65% of the *Kras* tumor mutations detected in VP-induced alveolar/bronchiolar carcinomas. Furthermore, the GAT and GTT mutations accounted for 9/25 (36%) and 1/25 (4%), respectively, of the *Kras* mutant alveolar/bronchiolar carcinomas from a pooled historical group of control mice. Consequently, these specific mutations are critical endpoints to examine in order to understand the MOA of VP-induced lung carcinogenesis.

The sensitivity of ACB-PCR should make it possible to ascertain how VP exposure affects the levels of these mutations in lung tissues following relatively short-term exposures to VP. ACB-PCR relies on the use of engineered mismatches within mutant-specific and blocker primers to selectively amplify mutant DNA sequence and repress amplification of the WT sequence in a PCR [8]. The mutant-specific primer is fluorescently-labeled, so amplification of mutant template DNA can be monitored as fluorescence of a product of the correct length. ACB-PCR is quantitative because a set of mutant fraction (MF) standards is analyzed in parallel with every set of unknown samples.

The following describes the work flow in an ACB-PCR analysis. Pure mutant and wild-type (WT) DNA sequences are synthesized *in vitro* from cloned plasmid DNAs

encompassing either the wild-type or mutant DNA sequence. All first-round amplifications are performed using a high-fidelity DNA polymerase (*PfuUltra* Hotstart DNA polymerase, with an estimated error rate of 4 X 10^{-7}). Genomic DNAs are isolated from the tissue samples of interest. Then, a first-round PCR product is synthesized from 1 μg of each DNA sample (3 x 10^5 molecules) using conditions that mitigate the potential for PCR-induced errors to influence the ACB-PCR measurement. Specifically, steps are taken to limit the amount of amplification to a level below that expected to produce PCR-induced errors at a level greater than 10^{-5}. The first-round PCR products generated from the lung DNA samples are identical in sequence composition to the MF standards. Purification of first-round PCR products is achieved using ion-paired reverse phase chromatography on the Transgenomic WAVE High Performance Liquid Chromatography System (Transgenomic Inc., Omaha NE). Many single-use aliquots of purified first-round PCR products and standards are prepared. The DNA concentrations of all samples are quantified repeatedly until three measurements that vary from the group mean by no more than a certain amount (5 or 10%) are obtained. The DNA concentration is then used to set up ACB-PCR reactions (MF standards and unknowns) each containing the same number of input DNA molecules. The DNA standards are prepared by mixing different ratios of mutant:WT sequence. Duplicate sets of MF standards are prepared, with mutant:WT ratios of 10^{-1}, 10^{-2}, 10^{-3}, 10^{-4} or 10^{-5}. ACB-PCR experiments always include replicate no-mutant controls (only wild-type DNA) and a no DNA control. The WT only control defines the technical background of the assay. Generally, a low level of amplification from the WT template is observed. Equal volumes of ACB-PCR products (MF standards and unknowns) are loaded onto a polyacrylamide gel and the pixel

intensities of the correct-sized bands are quantified. Three replicate ACB-PCR assays are performed. The MF standards are used to construct a standard curve relating input MF to fluorescence (in pixels). The MFs of the unknown samples are interpolated from their fluorescent intensities using the formula for the standard curve. The MF for a particular animal/tissue sample is derived as the arithmetic average of three independent ACB-PCR measurements. A geometric mean MF and a median MF is calculated for each treatment group. In datasets where samples possess MFs below the limit of accurate ACB-PCR quantification (10^{-5}), statistical significance is assessed using a non-parametric test (by comparing the prevalence of samples in different groups with a MF above and below the limit of detection or the average/median MF for all samples analyzed).

In a recent analysis of *KRAS* mutation in normal human lung tissue and lung adenocarinomas, the average r^2 values for sets of nine standard curves were 0.9936 (range 0.9876 to 0.9965) and 0.9945 (range 0.9905 to 0.9973) for the *KRAS* codon 12 GAT and GTT mutational analyses, respectively. The *KRAS* codon 12 GAT and GTT geometric mean MFs measured in normal human lung were 3.25×10^{-5} and 3.15×10^{-5}, respectively [9]. The average coefficient of variation for triplicate *KRAS* codon 12 GAT and GTT MF measurements was 32.41% and 29.17%, respectively. For three ACB-PCR datasets that measured *Kras* mutation in mouse lung, the coefficients of variation were 0.40, 0.74, and 0.80 for the triplicate *Kras* codon 12 GAT MF measurements, and 0.56, 0.80, and 0.94 for the triplicate *Kras* codon 12 GTT MF measurements [3].

ACB-PCR has been used to detect the early effects of carcinogen treatment and to characterize dose-response. In addition, ACB-PCR data can be integrated with other measured endpoints (*e.g.*, DNA adducts and neutral reporter gene mutations) to assess

whether data across endpoints supports a particular MOA. Studies documenting that ACB-PCR can detect early effects of carcinogens are quite important because temporality of key events is a major consideration in establishing MOA. Several studies demonstrate ACB-PCR was able to detect mutation induction either shortly after acute exposure to a carcinogen or following a short chronic exposure to a carcinogen. ACB-PCR was used to measure induction of *Kras* codon 12 TGT mutation in A/J mouse lungs harvested 4 weeks after receiving a single i.p. injection of benzo[a]pyrene (B[a]P) [10]. ACB-PCR was used to demonstrate that induction of *Hras* mutation occurred in kidney and forestomach of Hupki mice following 3 weeks of daily gavage with 5 mg/kg of aristolochic acid I (AAI) [11]. And, in a study employing a time course design, ACB-PCR was able to detect a significant increase in colonic *Kras* codon 12 GAT mutation in rats one week after receiving two doses of azoxymethane (rats received a total of 15 mg/kg, in two doses administered one week apart) [12]. Conversely, ACB-PCR was used to show that induction of a tumor-associated *p53* mutation is not an early event in formaldehyde-induced carcinogenesis of the rat nasal mucosa [13].

In a multi-endpoint study on the effects of inhaled ethylene oxide (EO), ACB-PCR measurement of *Kras* codon 12 GAT mutation was found to be among the most sensitive endpoints (codon 12 GTT and TGT were also measured) [3]. A significant induction of this mutation was detected following 4 weeks of exposure (6 hours/day, 5 days/week) to 50, 100 and 200 ppm, making it a more sensitive endpoint than micronucleus, COMET, *cII* mutation, and histopathology. The concentrations of EO that induced lung tumors in a mouse tumor bioassay were 50 and 100 ppm.

We proposed analyzing codon 12 GTT and GAT MFs in lung DNAs of B6C3F$_1$ mice as a means of evaluating potential MOAs for alveolar/bronchiolar tumorigenesis in VP-exposed mice. The first hypothesis is that VP induces *Kras* mutations via a direct oxidative effect on the guanine at the second position of codon 12. 8-Oxo-2'-deoxyguaninosine (8-oxo-dG), an oxidized form of deoxyguanosine, is a well-known marker of oxidative DNA damage, which causes A:T to C:G or G:C to T:A transversion mutations. Increases in 8-oxo-dG have been shown to occur in VP treated mouse lung [14]. If direct oxidation of *Kras* codon 12 (WT, GGT) is responsible for its carcinogenic effects, then induction of *Kras* codon 12 GTT mutation is expected to be an early event in VP-induced lung carcinogenesis, whereas no early increase in *Kras* codon 12 GAT mutation would be expected based on this potential MOA. A second hypothesis is that the VP MOA for lung carcinogenesis involves amplification of preexisting *Kras* mutations as an early key event. Evidence that VP inhalation induces *Kras* codon 12 GAT mutation to an equal or greater extent than *Kras* codon 12 GTT mutation would support amplification of preexisting mutation as an early key event in VP-induced lung carcinogenesis. In addition, a goal of this project was to investigate whether VP-induced oxidative stress could lead to non-monotonic changes in *Kras* MF, for example a mitogenic effect on *Kras* mutant cells at low VP concentration but induction of *Kras* mutant cell senescence or cell death at thigh VP concentration. A third hypothesis (associated with an unknown MOA) is that *Kras* mutation is a late event in VP-induced lung carcinogenesis and that no increase in *Kras* mutation would be detected after a short-duration exposure. In order to investigate these alternative hypotheses, male B6C3F$_1$ mice were exposed to particulate aerosols of VP using conditions that replicate

the tumor bioassay of VP, except using a shorter duration of exposure and using concentrations overlapping with the tumorigenic concentrations. Specifically, 6 male mice per treatment group were exposed via inhalation to aerosolized VP at concentrations of 0, 0.1, or 1 mg/m^3 VP for 6 hours/day, 6 days/week, for 4 and 8 weeks.

MATERIALS & METHODS

Animals and VP exposure

Investigators within the IIT Research Institute in Chicago, IL conducted the nose-only inhalation exposures of male Big Blue (BB) B6C3F$_1$ mice to VP and confirmed the accuracy of the exposure conditions. Male Big Blue (BB) B6C3F$_1$ mice (6 mice/group) were exposed to target concentrations of 0, 0.1, or 1.0 ppm VP by inhalation, 6 hours/day, 5 days/week for 4 or 8 weeks. Sham-exposed and VP-exposed mice were sacrificed, then lungs were removed and snap-frozen in liquid nitrogen. The left lobe of each mouse lung was shipped to NCTR on dry ice for ACB-PCR analysis of *Kras* mutation. Lung tissue samples were labeled: "2246 SN1 BBBigBlue MaleGroup 4WK #[sample number] Left Lung 11/11/2013" or "2246 SN1 BBBigBlue MaleGroup 8WK #[sample number] Left Lung 12/9/2013," and a treatment key was provided with each shipment. The samples were received in two separate shipments (corresponding to samples exposed for 4 or 8 weeks). Each sample was assigned an NCTR protocol 7229.21 sample number (1 through 36) as recorded in the Master Sample Sheet (see Appendix I, Table A1).

The IIT Research Institute provided Dr. Mugimane Manjanatha with tissue from the right side of the lungs of the same male Big Blue B6C3F$_1$ mice. Dr. Manjanatha measured *cII* mutant frequency in DNA isolated from the lung tissue of these mice and provided those measurements, enabling correlations between *cII* mutant frequency and *Kras* MF within individual animals to be determined.

Isolation of Lung DNA

Inhaled VP was expected to accumulate in the lung tissue. Therefore, the DNA isolation protocol was modified to limit the potential for DNA damage during the DNA isolation process. To isolate high-molecular weight genomic DNA, lung tissues were minced then homogenized in 1 ml of extraction buffer, consisting of 0.5 mg/ml proteinase K, 20 mM NaCl, 1 mM $CaCl_2$, pH 8.0, and 10 mM Tris pH 8.0. Samples were incubated for 3 hours at 37°C, then extracted with an equal volume of phenol/chloroform/isoamyl alcohol (25:24:1) and ethanol-precipitated. Samples were resuspended in 400 µl of RNase buffer: 10 mg/ml RNase A (Sigma, St. Louis, MO), 600 units/ml Ribonuclease T1 (Sigma), 100 mM sodium acetate, and 50 mM Tris-HCl (pH 8), incubated ~16 hours at 37 °C, then re-extracted with phenol/chloroform/isoamyl alcohol as described above. Each DNA sample was ethanol precipitated, then resuspended in 50 µl of TE buffer (5 mM Tris, 0.5 mM EDTA, pH 7.5). DNA samples were digested with HindIII according to the manufacturer's instructions (New England Biolabs, Beverly, MA). Finally, the DNA was phenol/chloroform/isoamyl alcohol extracted as described above, ethanol-precipitated and resuspended in 20 µl of TE buffer. DNA concentrations were measured spectrophotometrically, after which DNA

samples were diluted to 0.5 µg/ul and the DNA concentration was determined spectrophotometrically.

The isolation procedure produced high molecular weight DNA from all samples as determined by agarose gel electrophoresis, examining HindIII-digested and undigested DNA samples in adjacent wells (see Appendix II, Figure A1A).

Preparation of standards and unknowns by first-round PCR amplification

First-round PCR products were prepared from standards and unknowns as previously described [3]. A first-found PCR amplification, employing the *PfuUltra* hotstart high-fidelity DNA polymerase (Stratagene, La Jolla, CA) amplified a *Kras* gene sequence from linearized plasmid DNAs, in order to synthesize the MF standards. Similarly, HindIII-digested, lung DNA samples were used to amplify a *Kras* gene sequence for each mouse in the study (see Appendix II, Figure A1B). The PCR conditions for plasmid and genomic DNA amplification had been optimized previously, such that <0.8 µg of product was produced in a given PCR. This amount of product was less than that expected to be synthesized in 24 doublings of the input template (3 x 10^5 molecules). Using the formula $F(>1)=1-e^{-bfd}$, where b = the length of the target, f = the reported fidelity of *PfuUltra* hotstart high-fidelity DNA polymerase [4 x 10^{-7}/basepair (bp)], and d = the number of doublings, it was calculated that 24 doublings of input template molecules would induce errors at a frequency (9.6 x 10^{-6}) below that measurable by ACB-PCR. Thus, limiting the first-round PCR to 28 cycles was used to mitigate the effect of PCR-induced errors on the results.

HindIII-digested, lung DNA was used for first-round PCR amplification of a 170 bp gene segment encompassing part of the 5' untranslated region, exon 1, and part of intron 1 (NC_000072 Region: 29,950 to 30,119). Each 200 µl PCR reaction contained: 1 µg genomic DNA, 200 nM primer TR67 (TR67, 5'-TGGCTGCCGTCCTTTACAA-3'), 200 nM primer TR68 (TR68, 5'-GGCCTGCTGAAAATGACTGAGTATAAACTTGT-3'), 200 nM dNTPs, 1X *PfuUltra* reaction buffer, and 10 units *PfuUltra* hotstart high-fidelity DNA Polymerase (Stratagene, La Jolla, CA). Cycling conditions were 94°C for 2 min, followed by 28 cycles of 94°C for 1 min, 58°C for 2 min, 72°C for 1 min, followed by a 7 min extension at 72°C. Primers were purchased from Integrated DNA Technologies, Coralville, IA.

Purification of and quantification of PCR products

The PCR products (standards and unknowns) were purified by ion-pair reverse phase chromatography using a WAVE Nucleic Acid Fragment Analysis System (Transgenomic, Omaha, NE). PCR products were complexed with 0.1 M triethylammonium acetate (Buffer A: 0.1M TEAA) and bound to a DNASep column (containing C18 alkylated PS/DVB polymer). PCR products, input template, unincorporated nucleotides, and primers were eluted using a gradient of increasing acetonitrile concentration (Buffer B: 0.1 M TEAA, 25% acetonitrile), thereby separating nucleic acids by size/column retention time. A threshold collection method was used to collect the 170 bp PCR products based on their absorbance at 260 (measured with a UV detector at the appropriate retention time) into individual tubes in a chilled fraction collector. PCR products were evaporated to dryness using a Savant Speed-Vac

Concentrator (Model ISS110, Thermo Fisher Scientific, Rockville, MD). PCR products were resuspended in TE buffer and multiple 2-µl aliquots were prepared and stored at -80°C. Multiple aliquots were repeatedly quantified using an Epoch Micro-Volume Spectrophotometer System with a Take3 Microplate Reader (Biotek Instruments, Winooski, VT), until three measurements that varied by <5% (first determination/Experiment 1) or <10% (second determination/Experiment 2) from the group mean were obtained.

Previously prepared *Kras* codon 12 GAT and GTT mutant standards were available at the initiation of this project, but WT standard was not. Therefore, new WT standard was synthesized and isolated after which the 4-week and 8-week mouse samples were synthesized and isolated. When a higher than expected level of inter-sample variability was observed in the ACB-PCR analysis of MF, new *Kras* codon 12 GAT and GTT mutant standards were synthesized and purified.

ACB-PCR quantification of *Kras* codon 12 GAT and GTT MFs

Before the study was initiated, the sale of the Stoffel fragment of *Taq* polymerase (the enzyme used in ACB-PCR) by Stratagene (La Jolla, CA) was discontinued. Therefore, initial work investigated the utility of Tfi (Life Technologies, Grand Island, NY) and Hemo KlenTaq (New England Biolabs, Beverly, MA) DNA polymerases in ACB-PCR. After establishing that KlenTaq provided better results, the *Kras* codon 12 GAT and GTT ACB-PCR methodologies were re-optimized using the KlenTaq enzyme.

Purified mutant and WT first-round PCR products (generated using plasmid templates) were mixed to generate standards with MFs of 10^{-1}, 10^{-2}, 10^{-3}, 10^{-4}, 10^{-5}, and

0. Duplicate MF standards and a no-DNA control were analyzed in parallel with equal numbers of copies of first-round PCR products generated from mouse lung DNA samples. For the ACB-PCR analysis of both mutations, a total of 5×10^6 copies were analyzed in 50 µl reactions performed in 96-well plates using a DNA Engine Tetrad 2 (Bio-Rad Life Science Research, Hercules, CA).

For quantification of *Kras* codon 12 GAT mutation, each ACB-PCR reaction contained: 1X Standard *Taq* (Mg-free) reaction buffer (New England Biolabs), 0.1 mg/ml gelatin, 1 mg/ml Triton X-100, 40 µM dNTPs, 1.6 mM $MgCl_2$, 150 nM mutant-specific primer (TR76, 5'-fluorescein-CTTGTGGTGGTTGGAGCTAA-3'), 520 nM blocker primer (TR77, 5'-CTTGTGGTGGTTGGAGCTAdG-3'), and 150 nM upstream primer (TR73, 5'-TCGTAGGGTCGTACTCATC-3'). Each reaction was initiated with the addition of 1.2 units of Extreme Thermostable Single-stranded DNA Binding Protein, 0.33 mUnits of PerfectMatch PCR Enhancer, and 70 mUnits of Hemo KlenTaq DNA polymerase. Cycling conditions were 2 min at 94°C, followed by 36 cycles of 94°C for 30 sec, 45°C for 45 sec, and 72°C for 1 min. The *Kras* codon 12 GAT ACB-PCR product is 91 bp in length.

For quantification of *Kras* codon 12 GTT mutation, each ACB-PCR reaction contained: 1X Standard *Taq* (Mg-free) reaction buffer, 0.1 mg/ml gelatin, 1 mg/ml Triton X-100, 40 µM dNTPs, 1.5 mM $MgCl_2$, 400 nM mutant-specific primer (TR87, 5'-fluorescein-CTTGTGGTGGTTGGAGCTAT-3'), 440 nM blocker primer (TR113, 5'-CTTGTGGTGGTTGGAGCTTG-3'-phosporylation), and 400 nM upstream primer (TR110, 5'-TCGTAGGGTCATACTCATC-3'). Each reaction was initiated with the addition of 160 mUnits of PerfectMatch PCR Enhancer (Stratagene), and 80 mUnits of

Hemo KlenTaq DNA polymerase. Cycling conditions were 2 min at 94°C, followed by 36 cycles of 94°C for 30 sec, 41°C for 45 sec, and 72°C for 1 min. The *Kras* codon 12 GTT ACB-PCR product is 91 bp in length.

Gel electrophoresis and quantification of ACB-PCR products

Because each mutant-specific primer is labeled with a 5' fluorescein molecule, ACB-PCR products can be quantified based on the fluorescence of the correct-sized band following vertical polyacrylamide gel electrophoresis. Following ACB-PCR, 10 µl of bromophenol blue/xylene cyanol-containing 6X ficol loading dye was added to each well of the 96-well plate. Then, 15 µl of each *Kras* codon 12 GAT ACB-PCR reaction or 10 µl of each *Kras* codon 12 GTT ACB-PCR reaction were analyzed on 8% non-denaturing polyacrylamide gels. During the optimization, a fluorescent DNA length marker was used to confirm the identity of the 91-bp products. Fluorescent bands were visualized using a PharosFX scanner with an external blue laser (Bio-Rad). Pixel intensities of the bands were quantified using Quantity One® software and a locally-averaged background correction (Bio-Rad).

Data Analysis

The pixel intensities determined for the MF standards were plotted against their MFs on log-log plots. A trend line (power function) was fitted to the data and the formula of the function was used to calculate the MF in each unknown sample based on its pixel intensity. The arithmetic average of the three independent MF measurements was calculated. The average MF in each lung DNA sample was log-transformed and

the average log-transformed MF for the six mice in each treatment group was calculated. This value is the geometric mean MF for each treatment group.

If measurements in a particular treatment group were $>10^{-5}$, but not normally distributed, then a Kruskal-Wallis test was used to assess the statistical significance between treatment groups. When measurements were below the limit of accurate ACB-PCR quantification (10^{-5}), the statistical significance of treatment effects was performed by comparing the distribution of samples above and below 10^{-5} among treatment groups, using a Fisher's exact test. The Spearman correlation coefficient was used to determine whether the *Kras* codon 12 GAT and GTT MFs within particular mice were correlated, and whether mutant frequency at the *cII* locus and *Kras* MF within particular mice were correlated. Relationships between these variables were also visualized using linear regression analyses. All statistical analyses were performed using GraphPad Prism Version 5 (GraphPad Software, Inc., La Jolla, CA), two-sided tests, and a significance level of 0.05.

RESULTS

Tissue samples corresponding to the left lobe of control and treated mice were weighed before DNA isolation (see Appendix Table A1). Analysis of variance (ANOVA) detected no significant effect of treatment on left lobe weight (4-week samples, P = 0.3871; 8-week samples, P = 0.3349). Following DNA isolation, first-round PCR products encompassing *Kras* exon 2 sequences were generated. The first-round PCR amplification of the 36 study samples had similar yields. Aliquots of the standards and purified PCR products were quantified until 3 replicates that varied by no more than 5%

from the group mean were obtained. Using the measured DNA concentrations, ACB-PCR analysis was performed, with all 36 of the study samples included in each experiment. Three independent ACB-PCR measurements were collected on each sample; meaning the assays were performed on three separate aliquots of first-round PCR product, each conducted using a unique set of MF standards. Gel images for two of three replicate *Kras* codon 12 GAT and GTT ACB-PCR assays are shown in Figure 1A and 1B, respectively. Gel images with volume reports regarding pixel intensities for the *Kras* codon 12 GAT and GTT ACB-PCR measurements are provided in Appendices III and IV, respectively. The standard curves and calculation of *Kras* codon 12 GAT and GTT MFs from sample pixel intensities and the standard curves are provided in Appendix V and VI, respectively.

The average correlation coefficient for the *Kras* codon 12 GAT standard curves was 0.9408 (range 0.9330 to 0.9469, Appendix V). The coefficient of determination for the triplicate GAT MF measurements was 1.07. The average correlation coefficient for the *Kras* codon 12 GTT standard curves was 0.9747 (range 0.9709 to 0.9799, Appendix VI). The coefficient of determination for the triplicate GTT MF measurements was 0.85. The pixel intensities of the MF standards incorporated as part of each ACB-PCR assay are plotted in Figure 2A and 2B for the *Kras* codon 12 GAT and GTT, respectively.

The average *Kras* codon 12 GAT and GTT MF measurements for each sample are given in Appendices VII (Table A2) and VIII (Table A3) and are plotted in Figure 3A and 3B, with the error bars indicating the standard error of the mean (SEM). Summary data are provided in Tables 1 and 2, respectively. The frequency distribution of measurements in each treatment group for *Kras* codon 12 GAT MF measured in mice

treated for either 4 or 8 weeks are plotted in Figure 4A and 4B, respectively. The frequency distribution of measurements in each treatment group for *Kras* codon 12 GTT measured in mice treated for either 4 or 8 weeks are plotted in Figure 4C and 4D, respectively.

All ACB-PCR MF data were log-transformed. A normality test was performed on the log-transformed *Kras* codon 12 GAT and GTT MF data from the 4- and 8-week time points. The 4-week GAT and 8-week GTT MF measurements were not normally distributed (Kolmogorov-Sminov test). Because all the 4-week *Kras* codon 12 GAT MF measurements were $>10^{-6}$ and were not normally-distributed, analysis of statistical differences among this dataset was performed using the non-parametric Kruskal-Wallis test, with Dunn's post-test comparing all pairs of treatment groups. A statistically-significant difference in *Kras* codon 12 GAT MF was observed among treatment groups exposed to VP for 4 weeks ($P = 0.0163$), with a significant difference between the control group and the 0.1 mg/m^3 VP treatment groups, but with no significant difference between the control and 1 mg/m^3 treatment groups (Figure 4A). The 8-week *Kras* codon 12 GAT and both *Kras* codon 12 GTT datasets each included a significant portion of samples with MFs below 10^{-5}. Given the large number of non-detects, treatment effects within these datasets were analyzed based on the number of samples with MFs greater than and less than 10^{-5} using Fisher's exact test. No other significant differences among treatment groups were observed.

Synthesis of new mutant standards and repeat of ACB-PCR analysis

Although the 4-week 0.1 mg/m^3 VP treatment group had significantly greater levels of *Kras* codon 12 GAT mutation than controls the biological significance of this result was unclear given that the magnitude of the effect was small relative to the larger than usual variation among the *Kras* codon 12 GAT MF measurements. In a previous study, the coefficients of determination for *Kras* codon 12 GAT MF measurements were 0.40, 0.74 and 0.80 [3], whereas the coefficients of determination for the 4-week *Kras* codon 12 GAT MF measurements in the current study was 1.07. The wild-type standard had been prepared for the current study, but the *Kras* codon 12 GAT and GTT mutant standards used were those prepared from an earlier study. Because the integrity of the MF standard DNA was one potential source of assay variation, these standards were re-synthesized and purified. Additional WAVE-purified *Kras* PCR product generated from each lung DNA sample was available to dilute and aliquot. Aliquots of the standards and purified PCR products were quantified until 3 replicates that varied by no more than 10% from the group mean were obtained. Using the measured DNA concentrations, ACB-PCR analysis was performed, with all 36 of the study samples included in each experiment. The data generated represent a second independent measurement of *Kras* MF for each unknown samples (designated Experiment 2).

Three independent ACB-PCR measurements were collected on each sample. Gel images for two of three replicate *Kras* codon 12 GAT and GTT ACB-PCR assays are shown in Figure 5A and 5B, respectively. Gel images with volume reports regarding pixel intensities for the *Kras* codon 12 GAT and GTT ACB-PCR measurements are provided in Appendices IX and X, respectively. The standard curves and calculation of

Kras codon 12 GAT and GTT MFs from sample pixel intensities and the standard curves are provided in Appendix XI and XII, respectively. The average correlation coefficient for the *Kras* codon 12 GAT standard curves was 0.9496 (range 0.9435 to 0.9528, Appendix XI). The coefficient of determination for the triplicate GAT MF measurements in Experiment 2 was 0.71, which is consistent with previous analyses. The average correlation coefficient for the *Kras* codon 12 GTT standard curves in Experiment 2 was 0.9594 (range 0.9579 to 0.962, Appendix XII). The coefficient of determination for the triplicate GAT MF measurements in Experiment 2 was 0.82, which was quite similar to that observed in the initial determination (Experiment 1). The pixel intensities of the MF standards incorporated as part of each ACB-PCR assay are plotted in Figure 2C and 2D for the *Kras* codon 12 GAT and GTT, respectively. Figure 2 shows that re-synthesis of the mutant standards resulted in somewhat more consistent replicate standard curves, particularly for the *Kras* codon 12 GAT mutation.

The average *Kras* codon 12 GAT and GTT MF measurements for each sample in Experiment 2 are plotted in Figure 3C and 3D, with the error bars indicating the standard error of the mean (SEM). Summary data is provided in Tables 3 and 4, respectively. For Experiment 2, the frequency distribution of measurements in each treatment group for *Kras* codon 12 GAT and GTT are plotted in Figure 6. Figure 6 shows that the *Kras* codon 12 GAT MFs measured in Experiment 1 (Figure 6A) were generally greater and somewhat differently distributed compared to those measured in Experiment 2 (Figure 6B). The *Kras* codon 12 GTT MF measurements from the two different experiments appear to be quite similar, in that each dataset contains only a few samples with MFs $>10^{-5}$ (see Figure 6C and 6D). A statistical analysis was performed

in order to determine whether the replicate *Kras* codon 12 GAT datasets are significantly different. Because the log-transformed *Kras* codon 12 GAT MF measurements were not normally distributed, a Mann-Whitney Rank Sum test was used to establish that the two datasets were significantly different ($P < 0.001$, two-tailed test). The $\log_{10}$-transformed *Kras* codon 12 GTT MF measurements from both experiments were normally-distributed, with most of the measurements below the level of accurate ACB-PCR quantification (below 10^{-5}). Because both datasets had identical numbers of samples above and below 10^{-5}, these datasets are not significantly different.

Cumulative dose-response assessment

The median MF for each treatment group was plotted relative to its cumulative exposure in Figure 7. Cumulative exposure was calculated as the VP exposure concentration multiplied by the number of hours the mice were exposed (either 120 hours for 4-week treatments or 240 hours for 8-week treatments). Figure 7 indicates no apparent effects of cumulative dose, so no statistical analyses for trend were conducted.

Correlation between *Kras* codon 12 GAT and GTT MF measurements

The Spearman correlation coefficient for the two different *Kras* MF measurements within individual mice was determined. In the first dataset (Experiment 1), only 5 samples had measureable levels of both mutations and the two different MF measurements were not correlated ($r = 0.6000$, $P = 0.3500$). In the second dataset (Experiment 2), 7 samples had measureable levels of both mutations (*i.e.*, $>10^{-5}$) and the two mutations were correlated at the 0.1, but not the 0.05, confidence level ($r =$

0.7143, P = 0.0881). The relationship between MF measurements in the two datasets was visualized by linear regression analysis (see Figure 8).

No significant correlations were observed between *cII* mutant frequency and *Kras* MF.

DISCUSSION

The observation that *Kras* mutation is more prevalent in VP-induced mouse alveolar/bronchiolar carcinomas than in spontaneous historical alveolar/bronchiolar carcinomas [7] supports the idea that *Kras* mutation is important in the etiology of VP-induced mouse lung tumor development. This study focused on quantifying levels of *Kras* mutation in mouse lung tissues following relatively short-term exposures to inhaled particulate VP aerosols as an approach to investigate three alternative hypotheses regarding the influence of VP exposure on the level of *Kras* mutation. One hypothesis was that a significant increase in the *Kras* codon 12 GTT mutation, with a concomitant increase in G→T mutation in the *cII* neutral reporter gene, would be consistent with VP causing oxidative damage that results in G→T mutation. It was hypothesized that significant increases in both *Kras* codon 12 GAT and GTT mutations, relative to their spontaneous levels, along with no shift in the *cII* mutational spectrum, would be consistent with amplification of pre-existing *Kras* mutation, which could occur by a variety of different mechanisms. The result that there was no significant increase in the *Kras* codon 12 GAT mutation and few mouse lung samples with measureable levels of *Kras* codon 12 GTT mutation does not support either of these two hypotheses. Instead the lack of any detectable increase in either mutation is most consistent with the

hypothesis that an increase in *Kras* mutation is a late event in VP-induced mouse lung carcinogenesis.

This study involved two separate measurements of *Kras* codon GAT and GTT MFs on the same first-round PCR products generated from the lung DNAs of sham- and VP-exposed mice. The initial result was a statistically-significant increase in *Kras* codon 12 GAT MF in mice exposed to 0.1 mg/m^3 VP, but not 1.0 mg.m^3. The biological significance of this result was equivocal given the small variation (~2-fold) between treatment groups compared to the large technical variation (coefficient of determination was 1.07). No significant differences among treatment groups were observed in the repeat analysis. For the *Kras* codon 12 GAT MF measurement, the two datasets are significantly different, indicating that it would be inappropriate to combine the data. There are a number of reasons to conclude the second set of *Kras* codon 12 GAT MF measurements are more precise than the initial set of measurements. First, the coefficient of determination for the second *Kras* codon 12 GAT MF experiment (0.71) was consistent with previous ACB-PCR analyses, unlike the initial experiment (1.07). Second, the average r^2 value for the standard curves improved to a small extent in the second experiment (r^2 = 0.9496 versus r^2 = 0.9408). The improved reproducibility among the ACB-PCR MF standards in the second experiment is borne out by less spread in the replicate standard curves, particularly at low MFs (compare Figure 2 A and C).

There were a number of technical differences between the initial and repeat analysis. First, approximately two-year old MF standards were used in the initial analysis, whereas new MF standards were synthesized and purified for the second

analysis. In the initial analysis, measurement of the DNA concentration of the first-round PCR products was performed until three measurements that varied by less than 5% from the group mean were obtained. This approach was different from the 10% that had been used in the past. This was investigated as an approach to improve the performance of the assay. By discounting DNA concentration measurements that varied between 5% and 10% from the group mean, however, an unintended bias may have been introduced into the measurement of *Kras* MF. The fact that the *Kras* codon 12 GTT assay produced similar results in the two replicate experiments suggests that the *Kras* codon 12 GAT MF standard, rather than the difference in DNA quantification approach, may be responsible for difference between the replicate *Kras* codon 12 GAT results. If the *Kras* codon 12 GAT MF standards used in the initial experiment were compromised, this could account for both the irreproducibility among replicate assays, as well as the greater *Kras* codon 12 GAT MFs measured in the initial determination compared to the second experiment. For this reason (as well as the fact that a stronger correlation was observed between the *Kras* codon 12 GAT and GTT MF measurements $>10^{-5}$ in the second experiment), we conclude the initial determination of the *Kras* codon 12 GAT MF is less precise than the second determination and that overall the results indicate that VP had a negligible effect on *Kras* MF under the treatment conditions employed.

Because *Kras* mutation is detected at a greater frequency in VP-induced tumors than in pooled historical spontaneous tumors, it is likely that a positive selection for *Kras* mutant cells contributes to the development of VP-induced alveolar/bronchiolar carcinomas. The upregulation of mitogen activated protein kinase signaling observed in

VP-induced alveolar/bronchiolar carcinomas [15] is also consistent with *Kras* mutant cells having a positive selective advantage, but it is a formal possibility that *Kras* mutant cells may be more resistant to induced cell death than tumor progenitors lacking *Kras* mutation (*i.e.*, *Kras* wild-type cells carrying other genetic lesions). Finally, the lack of a VP effect on *Kras* mutation in the ACB-PCR assay is consistent with the idea that selection of *Kras* mutant cells requires long-term VP exposure and/or may be a late event in VP-induced mouse lung carcinogenesis. Several possibilities exist in this regard. Proliferation of *Kras* mutant cells may be driven by oxidative stress, which may not occur in the short-term, but which may arise as a consequence of chronic inflammation. Alternatively, *Kras* mutant cell proliferation may be driven through a mechanism mediated by chronic inflammation, unrelated to oxidative stress. Finally, chronic inflammation/oxidative stress may be necessary to drive the acquisition of additional genetic lesions that drive tumor progression in concert with *Kras* mutation, thereby explaining why amplification of *Kras* mutation is a late event in VP-induced mouse lung carcinogenesis.

This study focused on quantifying levels of *Kras* mutation in mouse lung tissues as a function of inhaled particulate VP aerosols because: 1) *Kras* mutation is more prevalent in tumors induced by such exposure than in spontaneous mouse lung tumors, and 2) *Kras* is mechanistically involved in cellular responses to oxidative stress and inflammatory processes, which are potential key events in VP-induced lung carcinogenicity. Oxidative stress can augment Ras signaling, which can modulate ROS production [16-25]. The strength and duration of ROS signaling can in turn impact cell fate [3]. The work of Shuler *et al.* [14], which reported that oxidative DNA lesions (8-

oxodeoxyguanosine DNA adducts) were significantly increased in female B6C3F$_1$/Hsd mice exposed to 1 or 4 mg/m^3 vanadium dust aerosol for 16 days, is consistent with the interpretation that VP is carcinogenic through an oxidative stress mediated pathway. Interestingly, no significant increases in 8-OHdG lesions were observed in the related study conducted by Wang *et al.* [28], where male mice were exposed to 1 mg/m^3 vanadium dust aerosol for 4 or 8 weeks.

In the mouse, VP induces pulmonary inflammation and promotes tumor development [7, 27]. Using transgenic mice lacking cyclooxygenases and intratracheal installation of 1 mg/ml VP in saline, Bonner *et al.* [28] showed: 1) that VP-induced inflammation involved increased production of cyclooxygenase-2 and prostaglandin E_2, as well as secretion of tumor necrosis factor-α (TNF- α) into bronchoalveolar lavage fluid resulting in lung fibrosis, and 2) that production of cyclooxygenase-2 and prostaglandin E_2 were necessary to resolve the inflammatory effects of VP. In colon cancer cells lines, it has been demonstrated that *KRAS* mutational status impacts the apoptotic response mediated by TNF- α and extracellular signal-related kinases (ERK) pathway activation [29]. Thus, the finding that *Kras* tumor mutation is correlated with increased mitogen activated protein kinase pathway activation could be consistent with either an oxidative stress/*Kras*-mediated mechanism or an inflammatory microenvironment/*Kras*-mediated mechanism [15].

One goal of this project was to investigate whether oxidative stress could lead to non-monotonic responses in *Kras* MF. Specifically, it was hypothesized that short-term or low-level oxidative stress might result in an early mitogenic stimulus of pre-existing *Kras* mutant cells, whereas prolonged or high-level oxidative stress might generate a

negative selection against *Kras* mutant cells. The hypothesized loss of *Kras* mutation could operate through oncogene-induced senescence, apoptosis, or another form of cell death. As mentioned above, the work of Shuler *et al.* [14], in which female B6C3F1/Hsd mice received nose-only exposures to 1 mg/m^3 VP, found evidence of oxidative DNA damage, meaning it also had the potential to induce oxidative stress. In the current work, because companion analyses failed to uncover evidence of oxidative stress (in terms of 8-OHdG or changes in gene expression), we conclude the hypothesis that oxidative stress can cause non-monotonic responses in *Kras* MF was not adequately tested under the study conditions employed.

We found higher spontaneous *Kras* codon 12 GAT MFs as compared to codon 12 GTT MFs in mouse lung, consistent with previous observations [3]. The fact that the two different mutations from VP-exposed treatment groups were correlated ($r = 0.7143$, significant at the 90% confidence level), is consistent with the idea that VP exposure causes clonal expansion of both mutations.

In summary, inhalation of aerosols of particulate VP for 4 or 8 weeks did not result in significant changes in levels of *Kras* codon 12 GAT or GTT mutation. The data support the idea that the accumulation of additional *Kras* mutants is not an early event, and/or that the proliferative advantage of *Kras* mutant clones requires either longer expression times or larger cumulative VP exposures. It is possible that *Kras* mutant cells do not undergo clonal expansion until other cooperating genetic lesions occur, either secondary to VP-induced inflammation or other as yet undetermined mechanisms. Therefore, the data do not provide support for either a direct genotoxic effect of VP on *Kras* in the context of the exposure conditions used, nor early amplification of pre-existing mutation as being involved in genesis of VP-induced mouse lung tumors.

REFERENCES

1 EPA US. Guidelines for Carcinogen Risk Assessment 2005.

2 McKinzie PB, Delongchamp RR, Chen T, Parsons BL. ACB-PCR measurement of K-ras codon 12 mutant fractions in livers of Big Blue(registered trademark) rats treated with N-hydroxy-2-acetylaminofluorene. *Mutagenesis* 21 (6), 391-397 (2006).

3 Parsons BL, Manjanatha MG, Myers MB, McKim KL, D. Shelton S, Wang Y *et al.* Temporal Changes in K-ras Mutant Fraction in Lung Tissue of Big Blue B6C3F1 Mice Exposed to Ethylene Oxide. *Toxicological Sciences* 136, 26-38 (2013).

4 Parsons BL, Myers MB, Meng F, Wang Y, McKinzie PB. Oncomutations as biomarkers of cancer risk. *Environmental and Molecular Mutagenesis* 51 (8-9), 836-850 (2010).

5 Parsons BL, Meng F. K-RAS mutation in the screening, prognosis and treatment of cancer. *Biomarkers in Medicine* 3 (6), 757-769 (2009).

6 Parsons BL, Manjanatha MG, Myers MB, McKim KL, Wang Y, Gollapudi BB *et al.* Induction of CII and k-ras mutation in lung dna of big blue mice exposed to ethylene oxide by inhalation. *Environmental and Molecular Mutagenesis* 53, S62 (2012).

7 NTP. Toxicology and Carcinogenesis Studies of Vanadium Pentoxide (CAS No. 1314-62-1) in F344/N Rats and B6C3F1 Mice (Inhalation Studies). In: U.S. Department of Health and Human Services NIoH (ed): Research Triangle Park, NC 2002.

8 Parsons BL, McKinzie PB, Heflich RH. Allele-specific competitive blocker-PCR detection of rare base substitution. *Methods in molecular biology (Clifton, NJ)* 291 (-), 235-245 (2005).

9 Myers MB, McKim KL, Meng F, Parsons BL. Low-frequency KRAS mutations are prevalent in lung adenocarcinomas. *Personalized Medicine*, (in press).

10 Meng F, Knapp GW, Green T, Ross JA, Parsons BL. K-Ras mutant fraction in A/J mouse lung increases as a function of benzo[a]pyrene dose. *Environmental and Molecular Mutagenesis* 51 (2), 146-155 (2010).

11 Wang Y, Arlt VM, Roufosse CA, McKim KL, Myers MB, Phillips DH *et al.* ACB-PCR measurement of H-ras codon 61 CAA->CTA mutation provides an early indication of aristolochic acid I carcinogenic effect in tumor target tissues. *Environmental and Molecular Mutagenesis* 53 (7), 495-504 (2012).

12 McKinzie PB, Parsons BL. Accumulation of K-Ras codon 12 mutations in the F344 rat distal colon following azoxymethane exposure. *Environmental and Molecular Mutagenesis* 52 (5), 409-418 (2011).

13 Meng F, Bermudez E, McKinzie PB, Andersen ME, Clewell HJ, Parsons BL. Measurement of tumor-associated mutations in the nasal mucosa of rats exposed to varying doses of formaldehyde. *Regulatory Toxicology and Pharmacology* 57 (2-3), 274-283 (2010).

14 Schuler D, Chevalier HJ, Merker M, Morgenthal K, Ravanat JL, Sagelsdorff P *et al.* First steps towards an understanding of a mode of carcinogenic action for vanadium pentoxide. *Journal of Toxicologic Pathology* 24 (3), 149-162 (2011).

15 Devereux TR, Holliday W, Anna C, Ress N, Roycroft J, Sills RC. Map kinase activation correlates with K-ras mutation and loss of heterozygosity on chromosome 6 in alveolar bronchiolar carcinomas from B6C3F1 mice exposed to vanadium pentoxide for 2 years. *Carcinogenesis* 23 (10), 1737-1743 (2002).

16 Lander HM, Hajjar DP, Hempstead BL, Mirza UA, Chait BT, Campbell S *et al.* A molecular redox switch on p21(ras). Structural basis for the nitric oxide-p21(ras) interaction. *Journal of Biological Chemistry* 272 (7), 4323-4326 (1997).

17 Boldogh I, Hajas G, Aguilera-Aguirre L, Hegde ML, Radak Z, Bacsi A *et al.* Activation of Ras signaling pathway by 8-oxoguanine DNA glycosylase bound to its excision product, 8-oxoguanine. *Journal of Biological Chemistry* 287 (25), 20769-20773 (2012).

18 Burhans WC, Heintz NH. The cell cycle is a redox cycle: Linking phase-specific targets to cell fate. *Free Radical Biology and Medicine* 47 (9), 1282-1293 (2009).

19 Finkel T. Signal transduction by reactive oxygen species in non-phagocytic cells. *Journal of Leukocyte Biology* 65 (3), 337-340 (1999).

20 Kodama R, Kato M, Furuta S, Ueno S, Zhang Y, Matsuno K *et al.* ROS-generating oxidases Nox1 and Nox4 contribute to oncogenic Ras-induced premature senescence. *Genes to Cells* 18 (1), 32-41 (2013).

21 Lee AC, Fenster BE, Ito H, Takeda K, Bae NS, Hirai T *et al.* Ras proteins induce senescence by altering the intracellular levels of reactive oxygen species. *Journal of Biological Chemistry* 274 (12), 7936-7940 (1999).

22 Mates JM, Segura JA, Alonso FJ, Marquez J. Intracellular redox status and oxidative stress: Implications for cell proliferation, apoptosis, and carcinogenesis. *Archives of Toxicology* 82 (5), 273-299 (2008).

23 Serrano M, Lin AW, McCurrach ME, Beach D, Lowe SW. Oncogenic ras provokes premature cell senescence associated with accumulation of p53 and $p16^{INK4a}$. *Cell* 88, 593-602 (1997).

24 Shaw AT, Winslow MM, Magendantz M, Ouyang C, Dowdle J, Subramanian A *et al.* Selective killing of K-ras mutant cancer cells by small molecule inducers of oxidative stress. *Proceedings of the National Academy of Sciences of the United States of America* 108 (21), 8773-8778 (2011).

25 Weyemi U, Dupuy C. The emerging role of ROS-generating NADPH oxidase NOX4 in DNA-damage responses. *Mutation Research - Reviews in Mutation Research* 751 (2), 77-81 (2012).

26 Wang YZ, Bonner JC. Mechanism of extracellular signal-regulated kinase (ERK)-1 and ERK-2 activation by vanadium pentoxide in rat pulmonary myofibroblasts. *American Journal of Respiratory Cell and Molecular Biology* 22 (5), 590-596 (2000).

27 Rondini EA, Walters DM, Bauer AK. Vanadium pentoxide induces pulmonary inflammation and tumor promotion in a strain-dependent manner. *Particle and Fibre Toxicology* 7, (2010).

28 Bonner JC, Rice AB, Ingram JL, Moomaw CR, Nyska A, Bradbury A *et al.* Susceptibility of cyclooxygenase-2-deficient mice to pulmonary fibrogenesis. *American Journal of Pathology* 161 (2), 459-470 (2002).

29 Kreeger PK, Mandhana R, Alford SK, Haigis KM, Lauffenburger DA. RAS mutations affect tumor necrosis factor-induced apoptosis in colon carcinoma cells via ERK-modulatory negative and positive feedback circuits along with non-ERK pathway effects. *Cancer Research* 69 (20), 8191-8199 (2009).

Table 1. *Kras* Codon 12 GAT MF (Experiment 1) Summary Data and Statistical Analysis

Weeks on Study	VP Treatment Group (mg/m^3)	Geomean MF	Median MF	Number of samples with MF < 10^{-5}	Number of samples with MF > 10^{-5}	Statistically Significant*
4	0.0	6.09×10^{-5}	6.48×10^{-5}	0	6	-
	0.1	1.76×10^{-4}	1.33×10^{-4}	0	6	Yes
	1.0	1.10×10^{-4}	9.46×10^{-5}	0	6	No
8	0.0	8.89×10^{-5}	9.44×10^{-5}	0	6	-
	0.1	1.18×10^{-4}	9.48×10^{-5}	0	6	No
	1.0	1.90×10^{-4}	1.43×10^{-4}	0	6	No

*Statistical analysis was performed on log-transformed data. Because the measurements in the 4-week 0.1 and 1.0 VP treatment groups were not normally distributed, the non-parametric Kruskal Wallis test for analysis of variance based on ranks was employed.

Table 2. *Kras* Codon 12 GTT MF (Experiment 1) Summary Data and Statistical Analysis

Weeks on Study	VP Treatment Group (mg/m^3)	Geomean MF	Median MF	Number of samples with MF < 10^{-5}	Number of samples with MF > 10^{-5}	Statistically Significant*
4	0.0	1.89×10^{-6}	1.90×10^{-6}	6	0	-
	0.1	6.89×10^{-7}	8.61×10^{-7}	6	0	No
	1.0	1.07×10^{-6}	1.07×10^{-6}	6	0	No
8	0.0	1.11×10^{-6}	8.53×10^{-7}	6	0	-
	0.1	7.17×10^{-7}	8.80×10^{-7}	5	1	No
	1.0	2.68×10^{-6}	2.09×10^{-6}	5	1	No

*Because the majority of measurements were below the limit of accurate quantification, Fisher's exact test was used to compare the number of samples greater than and less than 10^{-5}.

Table 3. *Kras* Codon 12 GAT MF (Experiment 2) Summary Data and Statistical Analysis

Weeks on Study	VP Treatment Group (mg/m^3)	Geomean MF	Median MF	Number of samples with MF < 10^{-5}	Number of samples with MF > 10^{-5}	Statistically Significant*
4	0.0	2.04×10^{-5}	2.07×10^{-5}	0	6	-
	0.1	2.97×10^{-5}	2.02×10^{-5}	1	5	No
	1.0	1.39×10^{-5}	1.38×10^{-5}	2	4	No
8	0.0	1.02×10^{-5}	9.43×10^{-6}	2	4	-
	0.1	8.67×10^{-6}	6.40×10^{-6}	4	2	No
	1.0	1.86×10^{-5}	1.99×10^{-5}	2	4	No

*Because a significant number of measurements were below the limit of accurate quantification, Fisher's exact test was used to compare the number of samples greater than and less than 10^{-5}.

Table 4. *Kras* Codon 12 GTT MF (Experiment 2) Summary Data and Statistical Analysis

Weeks on Study	VP Treatment Group (mg/m^3)	Geomean MF	Median MF	Number of samples with MF < 10^{-5}	Number of samples with MF > 10^{-5}	Statistically Significant*
4	0.0	6.49×10^{-6}	6.26×10^{-6}	6	0	-
	0.1	3.08×10^{-6}	5.92×10^{-6}	2	4	No
	1.0	7.49×10^{-6}	5.24×10^{-6}	5	1	No
8	0.0	3.22×10^{-6}	2.70×10^{-6}	6	0	-
	0.1	1.61×10^{-6}	2.11×10^{-6}	4	2	No
	1.0	2.44×10^{-6}	3.71×10^{-6}	4	2	No

*Because the majority of measurements were below the limit of accurate quantification, Fisher's exact test was used to compare the number of samples greater than and less than 10^{-5}.

Figure Legends

Figure 1. Replicate gel images of *Kras* codon 12 GAT (A) and GTT (B) ACB-PCR products.

Figure 2. Comparison of replicate standard curves. Pixels intensities of MF standards from the initial analysis of *Kras* codon 12 GAT (A) and GTT MFs (B) and re-analysis in experiment 2 for *Kras* codon 12 GAT (C) and GTT MFs (D) are shown.

Figure 3. Replicate ACB-PCR measurements of *Kras* codon 12 mutation. The initial analysis of *Kras* codon 12 GAT (A) and GTT MFs (B) and re-analysis in experiment 2 for *Kras* codon 12 GAT (C) and GTT MFs (D) are shown. In each case the average MF is plotted, with the error bars indicating the SEM. Data points in the shaded area are considered below the limit of accurate ACB-PCR quantification.

Figure 4. Analysis of the *Kras* codon 12 mutation by treatment group. The distribution of *Kras* codon 12 GAT MFs measured in lungs of mice exposed to varying concentrations of VP for 4 (A) or 8 weeks (B) are shown. The distribution of *Kras* codon 12 GTT MFs measured in lungs of mice exposed to varying concentrations of VP for 4 (C) or 8 weeks (D) are shown. For each treatment group, the horizontal bar indicates the geometric mean MF and the error bars indicate the SEM. The dashed horizontal line denotes the limit of accurate quantification (10^{-5}).

Figure 5. Replicate gel images of *Kras* codon 12 GAT (A) and GTT (B) ACB-PCR products from Experiment 2.

Figure 6. Re-analysis of the *Kras* codon 12 mutation by treatment group. For Experiment 2, the distribution of *Kras* codon 12 GAT MFs measured in lungs of mice exposed to varying concentrations of VP for 4 (A) or 8 weeks (B) are shown. The distribution of *Kras* codon 12 GTT MFs measured in lungs of mice exposed to varying concentrations of VP for 4 (C) or 8 weeks (D) are shown. For each treatment group, the horizontal bar indicates the geometric mean MF and the error bars indicate the SEM. The dashed horizontal line denotes the limit of accurate quantification (10^{-5}).

Figure 7. Cumulative dose-response assessment. (A) Change in *Kras* codon 12 GAT MF as a function of cumulative VP exposure, measured in experiment 1. (B) Change in *Kras* codon 12 GTT MF as a function of cumulative VP exposure, measured in experiment 1. (C) Change in *Kras* codon 12 GAT MF as a function of cumulative VP exposure, measured in experiment 2. (D) Change in *Kras* codon 12 GTT MF as a function of cumulative VP exposure, measured in experiment 2. 4-week exposures included a total of 120 exposure hours (20, 6-hour exposures), 8 week exposures included a total of 240 exposure hours (40, 6-hour exposures). Cumulative doses were calculated as exposure concentration x total exposure hours. Data points in the shaded area are considered below the limit of accurate ACB-PCR quantification.

Figure 8. Correlation between *Kras* codon 12 GAT and GTT MF measurements in individual mouse DNA samples. Data from MFs measured in the initial analysis (experiment 1) are shown in (A). Data from Experiment 2 are shown in (B). Only individual mouse samples that measureable levels of both mutations are plotted.

Figure 1.

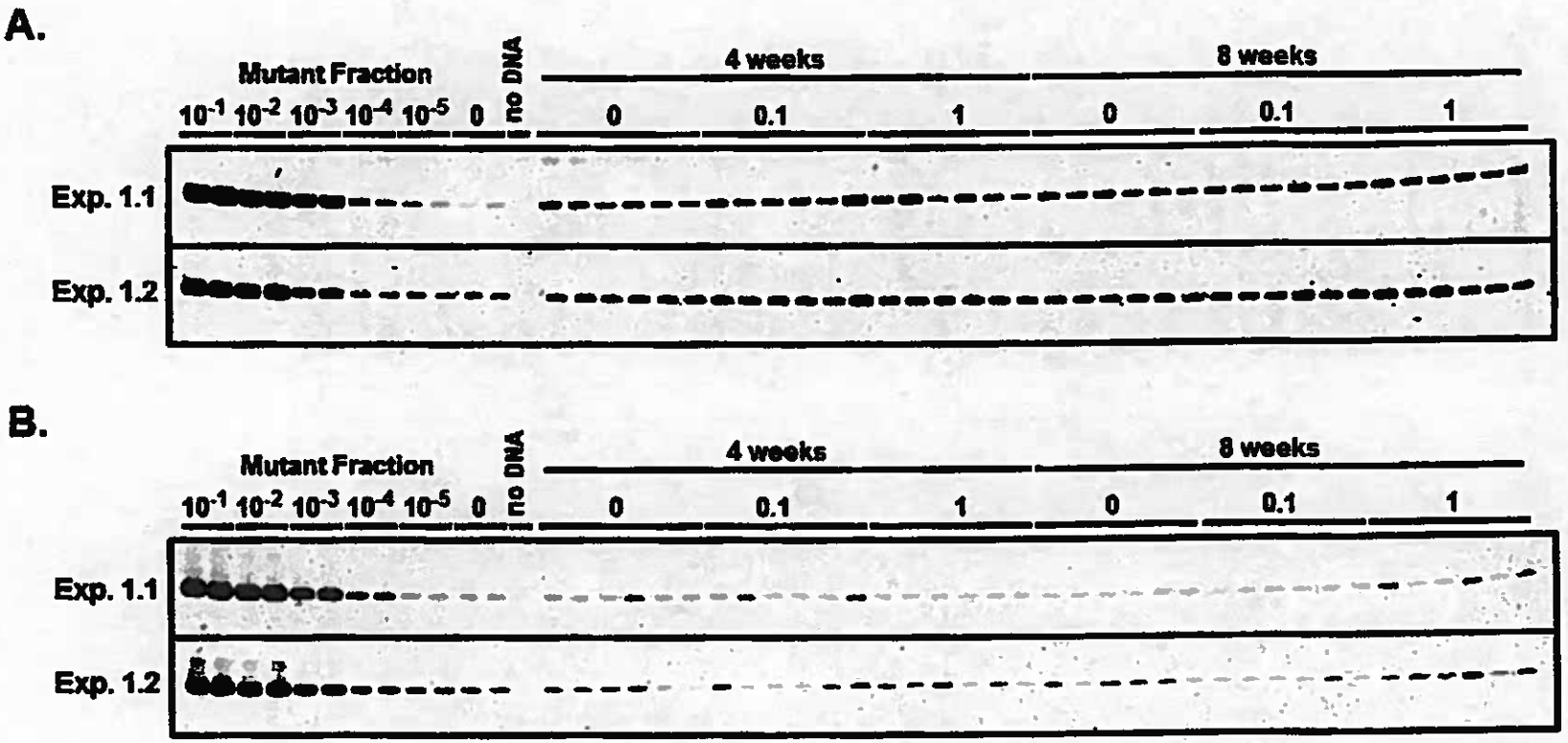
A.
Mutant Fraction
10-1 10-2 10-3 10-4 10-5 0
no DNA
4 weeks
8 weeks
0 0.1 1 0 0.1 1
Exp. 1.1
Exp. 1.2
B.
Mutant Fraction
10-1 10-2 10-3 10-4 10-5 0
no DNA
4 weeks
8 weeks
0 0.1 1 0 0.1 1
Exp. 1.1
Exp. 1.2

Figure 2.

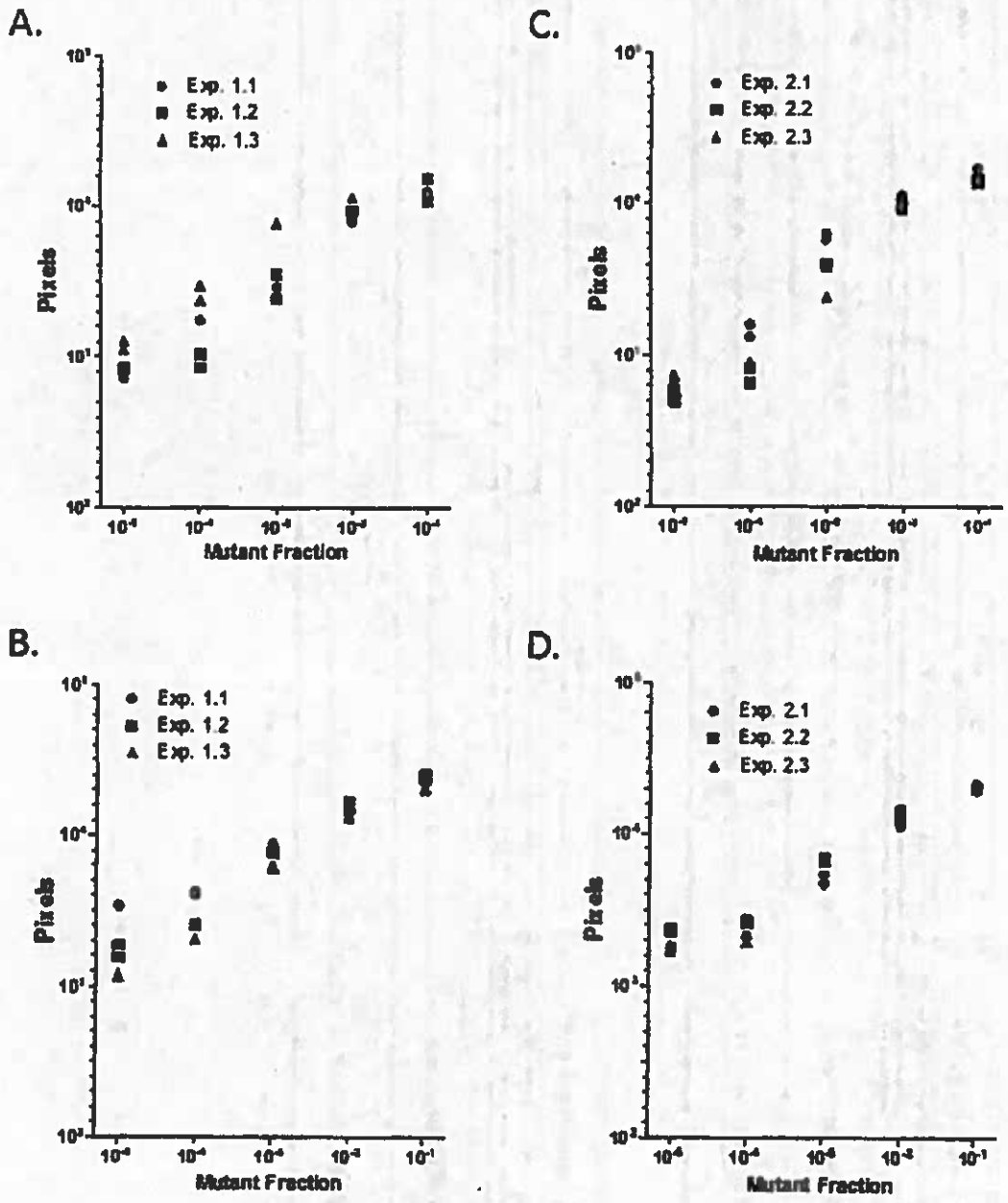
A.
Exp. 1.1
Exp. 1.2
Exp. 1.3
Pixels
Mutant Fraction
C.
Exp. 2.1
Exp. 2.2
Exp. 2.3
Pixels
Mutant Fraction
B.
Exp. 1.1
Exp. 1.2
Exp. 1.3
Pixels
Mutant Fraction
D.
Exp. 2.1
Exp. 2.2
Exp. 2.3
Pixels
Mutant Fraction

Figure 3.

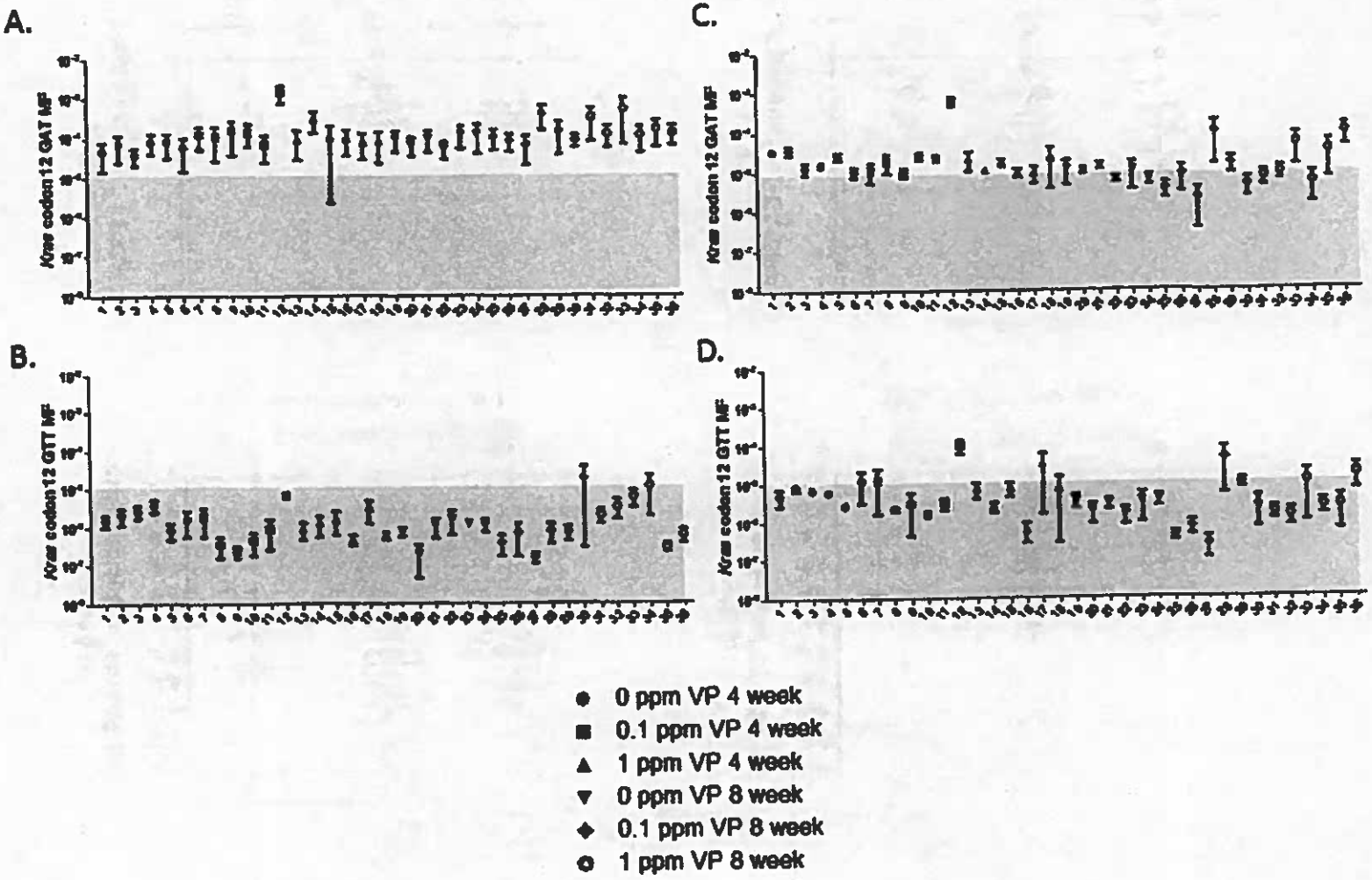
A.
C.
B.
D.
Kras codon 12 GAT MF
Kras codon 12 GTT MF
0 ppm VP 4 week
0.1 ppm VP 4 week
1 ppm VP 4 week
0 ppm VP 8 week
0.1 ppm VP 8 week
1 ppm VP 8 week

Figure 4.

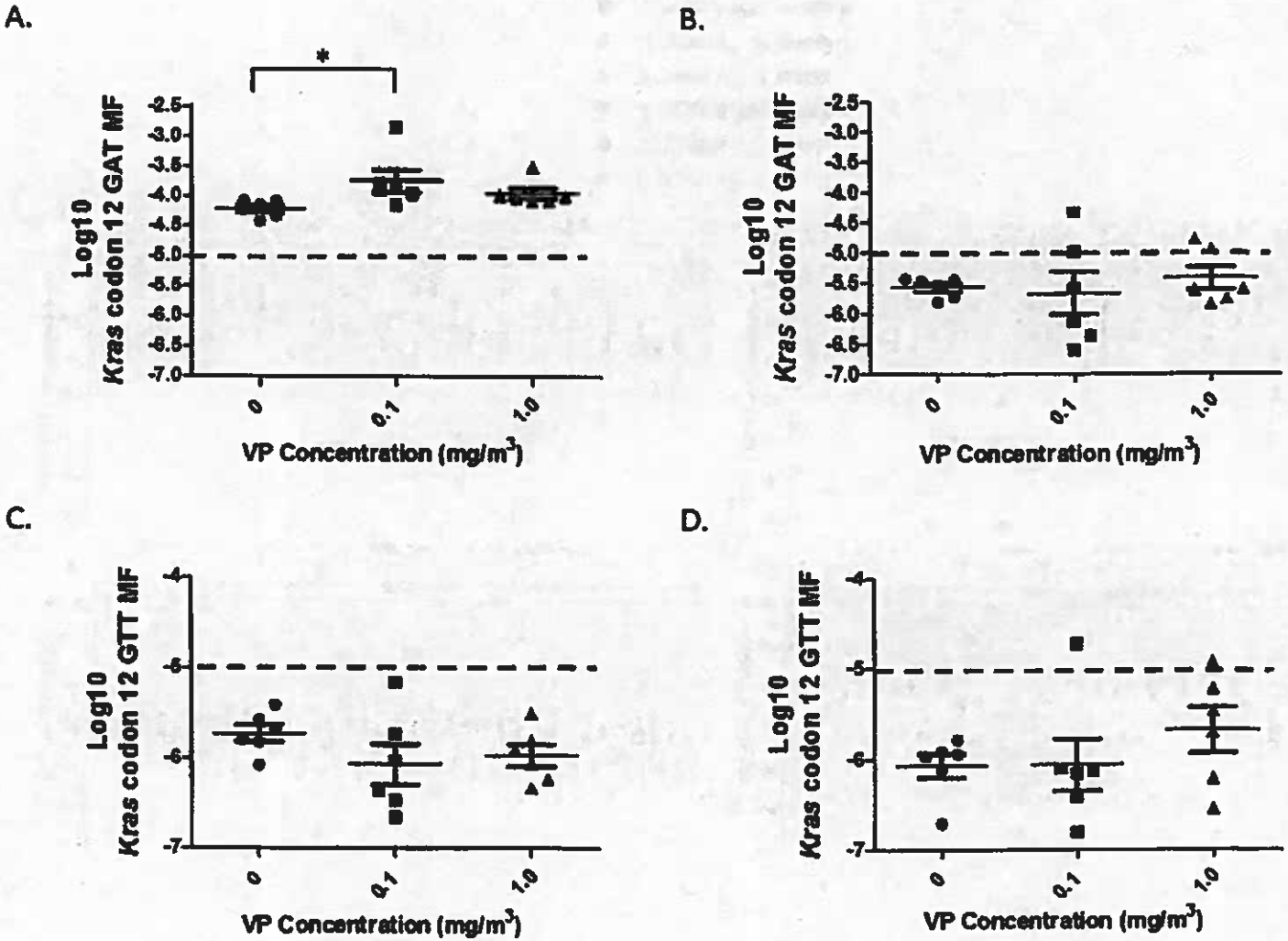
A.
B.
C.
D.
Log10 Kras codon 12 GAT MF
Log10 Kras codon 12 GTT MF
VP Concentration (mg/m3)
0
0.1
1.0
*

Figure 5.

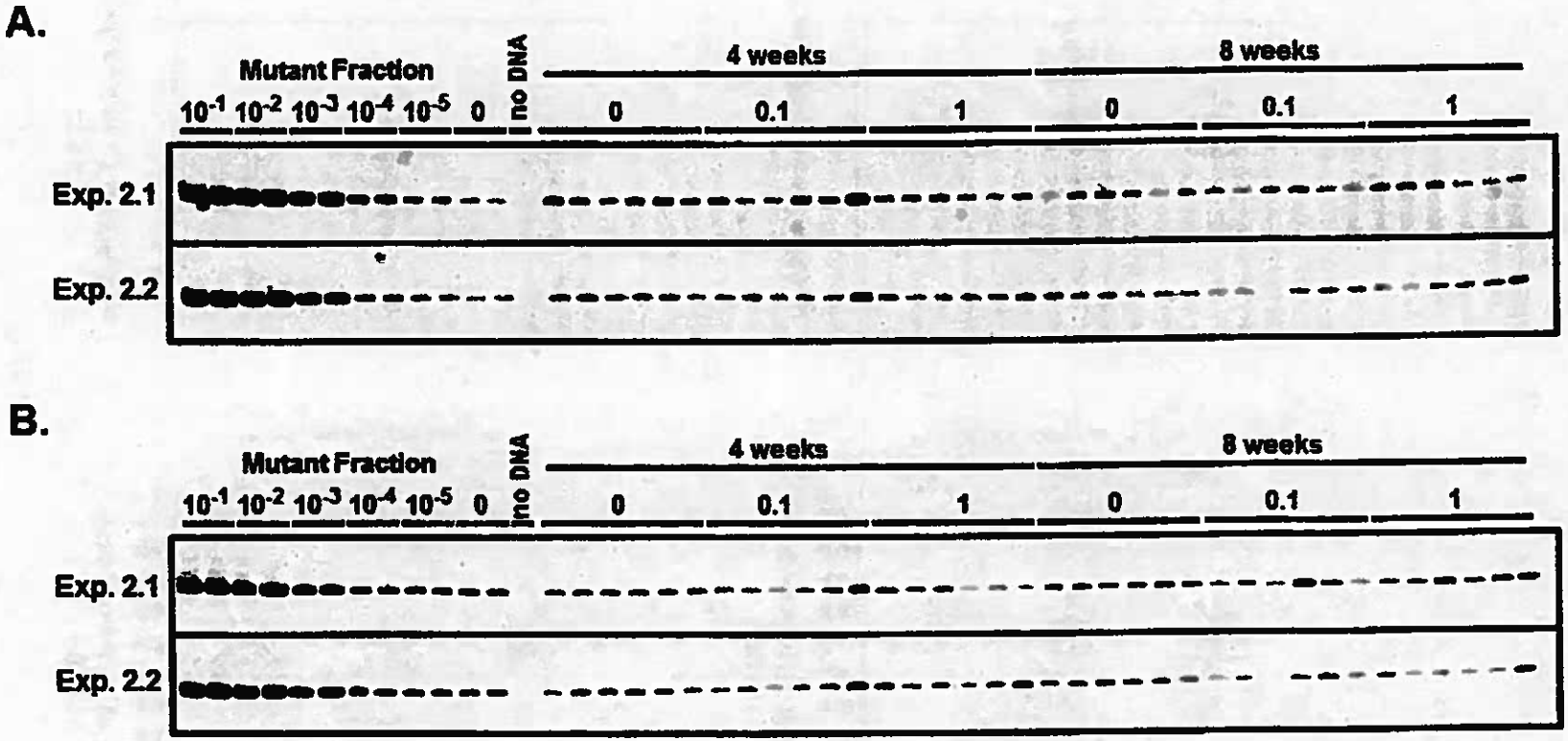
A.
Mutant Fraction
10-1 10-2 10-3 10-4 10-5 0
no DNA
4 weeks
8 weeks
0 0.1 1 0 0.1 1
Exp. 2.1
Exp. 2.2
B.
Mutant Fraction
10-1 10-2 10-3 10-4 10-5 0
no DNA
4 weeks
8 weeks
0 0.1 1 0 0.1 1
Exp. 2.1
Exp. 2.2

Figure 6.

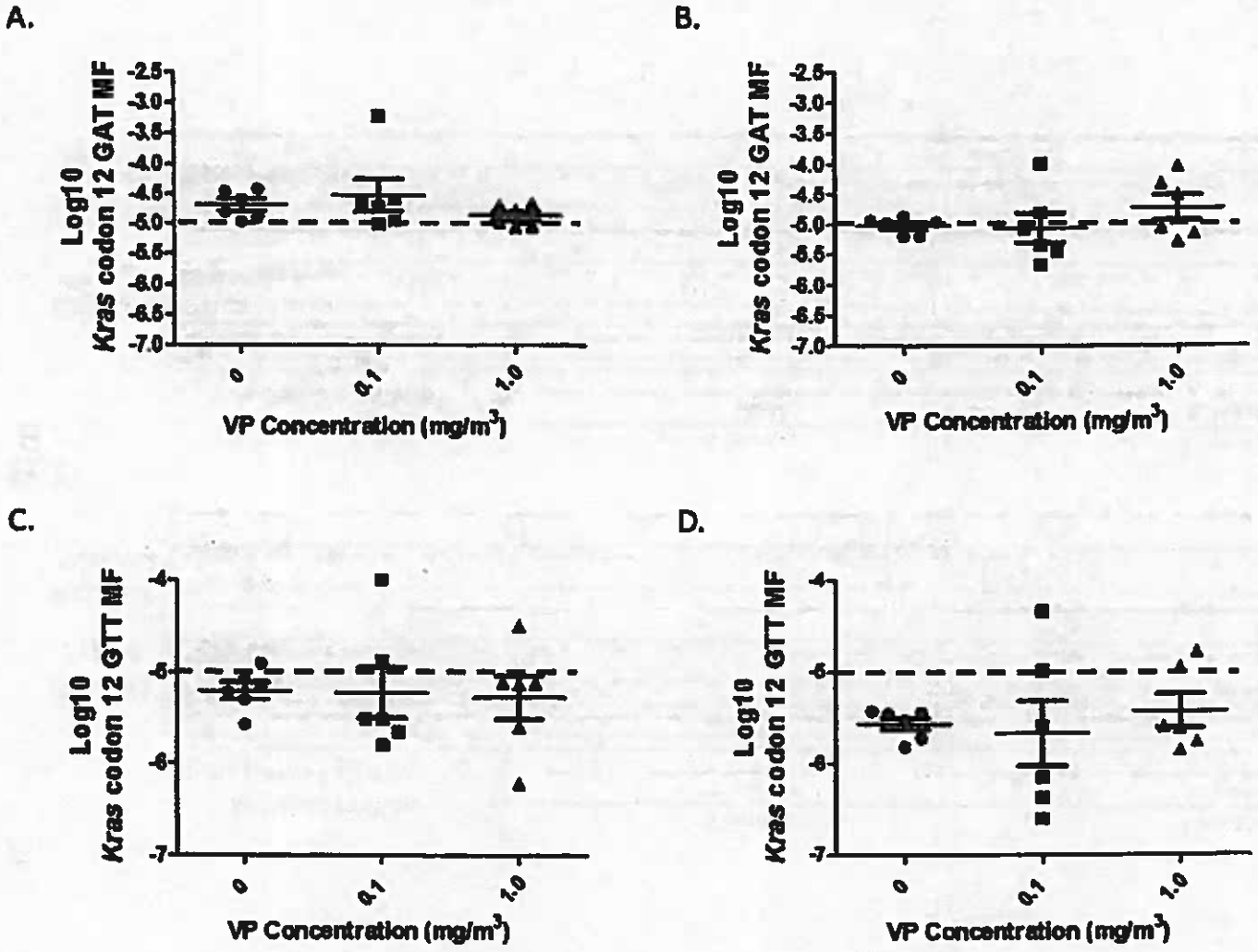
A.
B.
C.
D.
Log10 Kras codon 12 GAT MF
Log10 Kras codon 12 GTT MF
-2.5
-3.0
-3.5
-4.0
-4.5
-5.0
-5.5
-6.0
-6.5
-7.0
-4
-5
-6
-7
0
0.1
1.0
VP Concentration (mg/m3)

Figure 7.

A.

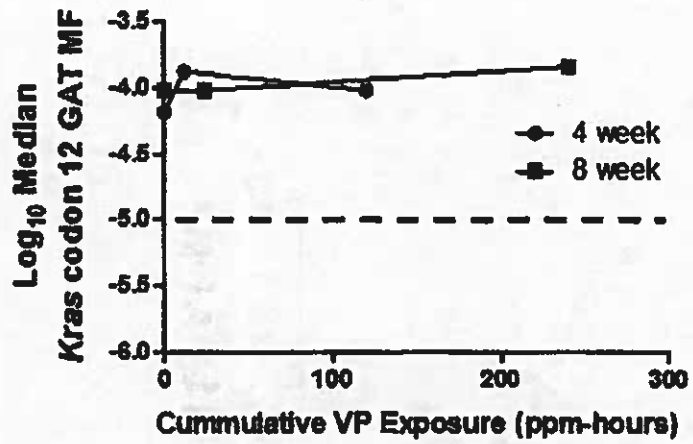

C.

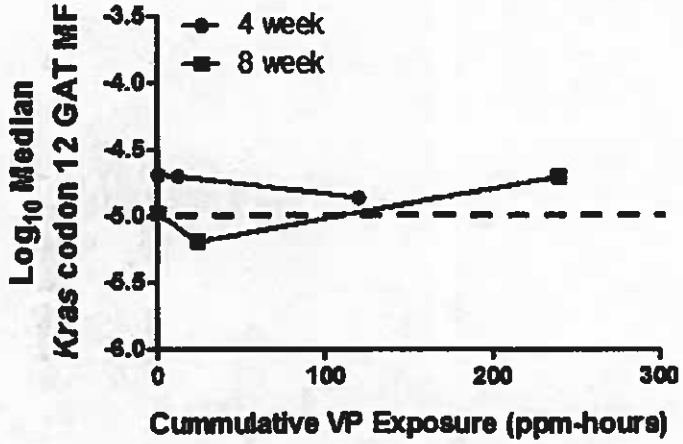

B.

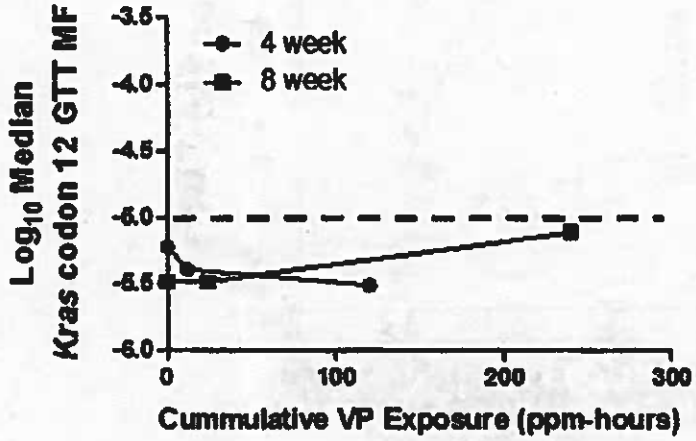

D.

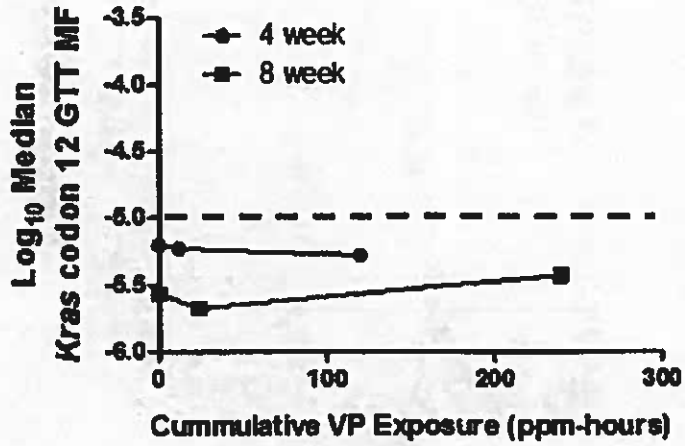

Figure 8.

A.

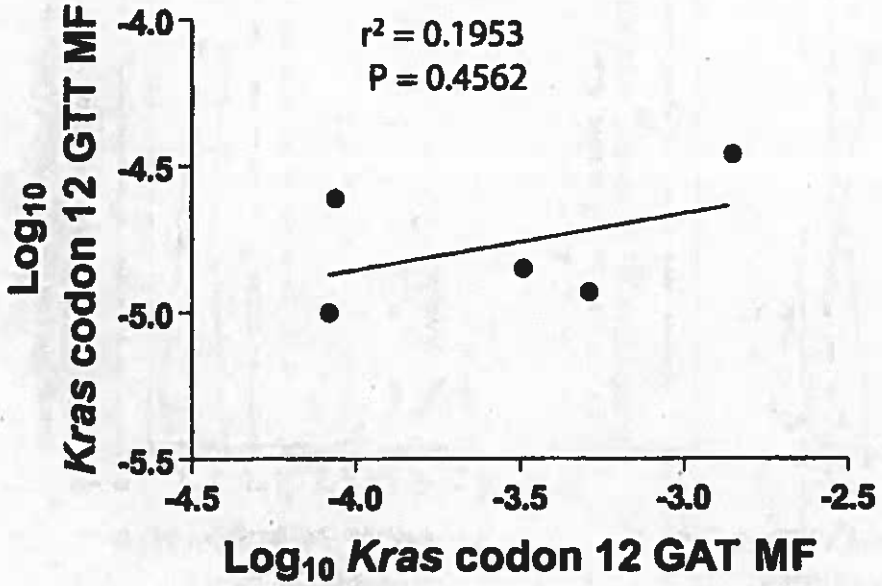
r² = 0.1953
P = 0.4562
Log10 Kras codon 12 GTT MF
-4.0
-4.5
-5.0
-5.5
-4.5
-4.0
-3.5
-3.0
-2.5
Log10 Kras codon 12 GAT MF

B.

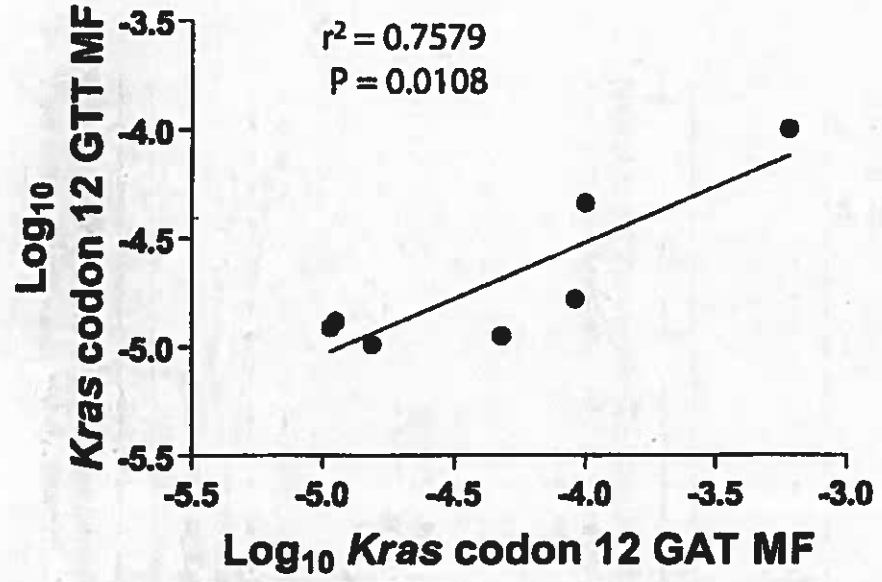
r² = 0.7579
P = 0.0108
Log10 Kras codon 12 GTT MF
-3.5
-4.0
-4.5
-5.0
-5.5
-5.5
-5.0
-4.5
-4.0
-3.5
-3.0
Log10 Kras codon 12 GAT MF